Electronic Supplementary Material (ESI) for Chemical Communications.

Supporting Information

A SIFSIX-MOF Constructed from a Metalloligand Yields Enhanced Stability for Selective CO_2 Adsorption

Alberto M. Tous-Granados and Arturo J. Hernández-Maldonado*

Department of Chemical Engineering, University of Puerto Rico-Mayagüez Campus Mayagüez, PR 00681-9000

* To whom correspondence should be addressed:

Phone: 787-832-4040 x3748; Fax: 787-834-3655; E-mail: arturoj.hernandez@upr.edu

---

Contents:

EXPERIMENTAL DETAILS

Reagents and materials. All reagents and chemicals were of analytical grade, used as received, and obtained from commercial suppliers. Copper(II) nitrate hemi(pentahydrate) ($Cu(NO_3)_2 \cdot 2.5H_2O$, 98%), copper (II) oxide (CuO, 99%), sodium sulfate (Na_2SO_4, 99%), sodium bicarbonate ($NaHCO_3$, 99.5%), *bpy* = 4,4′−bipyridine ($C_{10}H_8N_2$, 98%), MeOH (99.8%), chloroform ($CHCl_3$, 99%), toluene ($C_6H_5CH_3$, 99.5%), diethyl ether ($C_4H_{10}O$, 99%), tetrahydrofuran (C_4H_8O, 99%), and fluosilicic acid (H_2SiF_6, 35%) were obtained from Sigma-Aldrich. Acetyl chloride (CH_3COCl, 99%), 4-picoline (C_6H_7N, 99%), and *N*, *N*-dimethylacetamide ($CH_3CON(CH_3)_2$, 99%) were acquired from ACROS Organics™. Ultrahigh purity grade gases (Praxair, Inc.) were used for all measurements.

CAUTION! *The fluosilicic acid solution is toxic and corrosive to glass. Therefore, we strongly encourage the scientific community to follow the corresponding Safety Data Sheets (SDSs).*

Synthesis of 3-(4-pyridyl)pentane-2,4dione (H*pyac*). The organic ligand 3-(4-pyridyl)pentane-2,4dione (H*pyac*) was synthesized by slight adaptation of the procedures reported elsewhere (see Scheme S1 (A)).[1-2] In a typical synthesis, 4-picoline (39.1 g, 420 mmol) was added dropwise under an N_2 atmosphere to a previously cooled (-20 °C, *N*, *N*-dimethylacetamide-solid CO_2 slush bath) solution of acetyl chloride (26.3 g, 335 mmol) and $CHCl_3$ (150 mL). Stirring and cooling were continued for at least 3 hours, followed by vacuum distillation at 50 °C until a solid was obtained. Toluene (260 mL) was added under N_2 atmosphere, stirring was continued for at least 5 hours, and the slurry was filtrated. The filtrate was washed with DI water (3x20 ml) and dried with anhydrous Na_2SO_4 overnight. The final H*pyac* material was obtained upon vacuum distillation at 45 °C followed by slow room temperature crystallization (yield = 11.92 g).

Synthesis of bis[3-(4-pyridyl)pentane-2,4-dionato]copper(II) (Cu(*pyac*)$_2$). The copper metalloligand Cu(*pyac*)$_2$ was prepared following available procedures reported elsewhere (see Scheme S1 (B)).[3]

Synthesis of $CuSiF_6$. The anhydrous salt $CuSiF_6$ was prepared following recipes reported elsewhere.[4]

Synthesis of [Cu(*bpy*)$_2$(SiF_6)·xH_2O]$_n$. The [Cu(*bpy*)$_2$(SiF_6)·xH_2O]$_n$ variant also known as SIFSIX-1-Cu was synthesized following the procedure reported elsewhere.[5]

Synthesis of [Cu(Cu(*pyac*)$_2$)$_2$(SiF_6)·5H_2O]$_n$. A solution of $CuSiF_6$ (0.041 g, 0.20 mmol) in 80 ml of MeOH was dropwise added to a solution of Cu(*pyac*)$_2$ (0.166 g, 0.40 mmol) in 80 ml of tetrahydrofuran while stirring at room temperature for at least one minute. The blue precipitate was isolated by filtration and exchanged with MeOH at 55 °C for three days (2 times per day). Then the resulting powder was dried in *vacuo* at 50 °C overnight. Yield 0.085 g (72%).

Structure Elucidation. Powder X-ray diffraction (XRD) patterns of the samples were carried out on an X-ray diffractometer (ULTIMA III, Rigaku Corp.) fitted with cross beam optics (Cu Kα, 40kV, 44mA, λ = 1.54180 Å, 2 – 40 ° (2θ), step 0.02°, scan speed 0.1 to 1 °/min). Indexing was performed with an automatic peak search function and the dichotomy method of the PreDICT software suite.[6] A Le Bail structureless extraction was performed to refine the unit cell parameters and for the space group determination. GSAS-II was used to refine the structural model by the Rietveld technique using bonds, angles, and rigid body restraints.[7] The optimal positions of the hydrogen atoms were automatically located, and the thermal parameters of all atoms were refined isotropically. In addition, a spherical harmonics model was implemented to account for the

preferred orientation of the crystals in GSAS-II. It is worth noting that higher symmetry, *P* 2 / *m* (#10), was also tested during the structural refinement, and it was found feasible to represent the structure (see Table S2). However, a high level of disorder of both the carbon atoms of the pyridyl rings and the hydrogen atoms of methyl groups was detected with *P* 2 / *m* (#10) compared to *P* 2 (#3). For this reason, the *P* 2 (#3) monoclinic spacegroup was ultimately selected, which avoids the disorder of atoms and is a chemically plausible model of the new compound.

Single Component Gas Adsorption Measurements. The pure component adsorption isotherms were gathered with Micromeritics volumetric adsorption instruments (ASAP2020 for low pressure (< 1atm) and ASAP2050 for higher pressures (< 9 atm)). Prior to the adsorption measurements, the samples (~60 mg) were outgassed under vacuum (< 5 μmHg) at 50 °C for at least 4 hours. Free space and adsorption were analyzed at cryogenic temperatures with cooling baths (-196 °C with a liquid N_2 and -78 °C with Acetone/CO_2). For temperatures in the 25 to 45 °C range, the sample temperature was controlled using a heat blanket with automatic control. The equilibration time interval t_e (seconds), defined as the time between successive pressure readings required to reach an apparent equilibrium state or near-zero slope (e.g., for t_e = 100 sec, a time of about 1000 sec is required per pressure step), was 10-20 sec for measurements in the ASAP 2020 and between 20-100 sec for the ASAP2050.

Thermogravimetric Analysis. Thermogravimetric measurements (TGA) were executed with a TA-Q500 unit while heating the samples (~10 mg) of the as-synthesized materials from 20−900 °C, under N_2 atmosphere at 10 °C min^{-1}.

CALCULATION DETAILS

Textural Properties, Isosteric Heat, and Selectivity Calculations. N_2 (@-196 °C) and CO_2 (@-78 ° C) equilibrium adsorption isotherm data were used to estimate surface area (BET) and other porosimetry characteristics of the materials. A Horvath−Kawazoe model (HK-CY) based on slit-shaped pores with the Cheng-Yang correction was used to estimate a pore size distribution (PSD).[8] The micropore volume was estimated by applying the Modified Dubinin-Astakhov (MDA) (Equation S1) model to the CO_2 desorption legs and assuming that the phase packing of adsorbed molecules was similar to that of the liquid (see Table S1).[9] The MDA model was considered to account for possible deviations of the DA model from Henry's law.

$$q_{MDA} = q_o\{\beta_1 \exp[-(C \ln(P_0/P))^n] + \beta_2 KP\} \quad \text{(S1)}$$

where

$$\beta_1 = 1 - \exp\left(-\alpha \frac{P}{P_0}\right)$$

$$\beta_2 = \exp\left(-\alpha \frac{P}{P_0}\right)$$

$$C = \frac{RT}{\beta E}$$

$$C = \frac{q_1}{P_0}$$

q_{DA} or q_{MDA} is the adsorbed amount for each model, q_o is the saturated adsorbed amount (i.e., the pores are filled), E is adsorption energy, β is the affinity coefficient of the adsorbate, R is the universal gas constant, P/P_0 is the relative pressure, α is a fitting parameter, K is Henry's law constant, and n is the heterogeneity coefficient.

For the calculation of heat of adsorption $-\Delta H_{\text{ads}}$ (kJ mol^{-1}) for CO_2 over the PCPs, the Clausius-Clapeyron approach (Equation S2) was used with a direct polynomial fitting of the adsorption isotherms collected for three different but close temperatures $\Delta T \approx 10$ °C:

$$-\Delta H_{\text{ads}} = -RT^2 \left(\frac{\partial \ln P}{\partial T}\right)_n \quad \text{(S2)}$$

where $P(\text{atm})$ is pressure, $T(\text{K})$ is the temperature, n (mmol/g) is the adsorbed quantity, and R is the universal gas constant.[10] The temperatures selected for the single-component adsorption isotherms were 25, 35, and 45 °C. The isosteres plot of $\ln P$ Vs. $1/T$ was evaluated at different adsorbed amounts and yielded the heat of adsorption using equation S2).

The molar-based selectivity coefficient calculations were performed following the Myers and Prausnitz Ideal Adsorbed Solution Theory (IAST).[11] The single-component CO_2 and CH_4 adsorption isotherms that were gathered at 25 °C (see Figure S4) were first fitted (see Table S4) to the Dual-Site Langmuir-Freundlich (DSLF) model (Equation S3):

$$q = \frac{q_{sat,A} b_A p^{\alpha_A}}{1 + b_A p^{\alpha_A}} + \frac{q_{sat,B} b_B p^{\alpha_B}}{1 + b_B p^{\alpha_B}} \quad \text{(S3)}$$

where q is the adsorbed amount (mmol g^{-1}), q_{sat}(mmol g^{-1}) is the adsorbed amount at saturation, p (atm) is the gas pressure, b (atm^{-1}) and α (dimensionless) are the Langmuir-Freundlich adsorption parameter and exponent, respectively (A and B denote the two different adsorption sites). This model was employed due to the expected heterogeneity of the PCPs surfaces, particularly in the bimetallic variant.

IAST implies Raoult's equilibrium behavior between the adsorbent and the adsorbed phase, as shown in Equation S4:

$$P_i = P y_i = P_i^0 x_i \quad \text{(S4)}$$

$$\sum_{i=1}^{n} x_i = \sum_{i=1}^{n} \frac{P_i}{P_i^0} = 1 \quad \text{(S5)}$$

where P_i (atm) is the partial pressure of component *i*, *P* (atm) is the total overhead pressure of the mixture, where x_i and y_i are the mole fraction of component *i* in the adsorbed and bulk phases,

respectively. IAST requirement is that the spreading pressures of all components must be equal at constant *T*, which after analytical integration of the DSLF model yields (Equation S6):

$$\int_0^{P_i^0} \frac{q_i(P_i)}{P_i} dP_i = \Pi(Constant) = \frac{q_{sat,A}}{\alpha_A} ln[1 + b_A(P_i^0)^{\alpha_A}] + \frac{q_{sat,B}}{\alpha_B} ln[1 + b_B(P_i^0)^{\alpha_B}] \quad \text{(S6)}$$

For a CO_2 (Component 1) and CH_4 (Component 2) binary system, the IAST selectivity coefficient (Equation S8) can be obtained by simultaneously solving equations (5) and (6) for the unknowns Π, P_1^0, and P_2^0.

$$S_{\text{IAST}} = \frac{x_1/y_1}{x_2/y_2} \quad \text{(S7)}$$

Table S1. Crystallographic data and Rietveld refinement summary for $[Cu_2(Cu(pyac)_2)_2(SiF_6)]_n$ without guest molecules.

formula	$C_{40}H_{40}Cu_3F_6N_4O_8Si$
formula wt.	1037.50
ρ (g cm^{-3})	0.637
crystal system	monoclinic
space group	*P* 2 (#3)
a (Å)	19.035(7)
b (Å)	8.059(1)
c (Å)	19.065(5)
β (°)	112.48(1)
V (Å^3)	2702.58(0)
Z	1
diffractometer	Bragg-Brentano
X-ray source	CuKα
wavelength (Å)	1.54180
step (°)	0.01
2θ range (°)	2 – 50
R_I [a]	0.22285
R_{wp} [b]	0.15463

[a] $R_{wp} = \left[\sum_i w_i\left(y_{C,i} - y_{O,i}\right)^2 / \sum_i w_i\left(y_{O,i}\right)^2\right]^{1/2}$, [b] $R_I = \sum_i \left|I_{O,i} - I_{C,i}\right| / \sum_i I_{O,i}$

Note: The quality of the Rietveld fit was assessed through numerical values of the Rietveld errors (i.e., R_I and R_{wp}) and a graphical plot of observed and calculated patterns (see Figure S1) to ensure that the model is chemically plausible.[12]

Table S2. Atomic coordinates for $[Cu_2(Cu(pyac)_2)_2(SiF_6)]_n$ for the trial solution using the spacegroup *P* 2 / *m* (#10).

Atom	*x*	*y*	*z*
Cu1	0.00000	0.00000	0.00000
Si1	0.00000	0.50000	0.00000
F1	0.00000	0.29490	0.00000
F2	-0.06386	0.50000	0.04285
F3	0.06799	0.50000	0.08219
F4	0.00000	0.70510	0.00000
Cu2	0.00000	0.00000	0.50000
O1	-0.07306	0.00000	0.41009
O2	0.08111	0.00000	0.45973
C1	0.14124	0.00299	0.37458
H1	0.18081	0.05585	0.41625
H2	0.13215	0.06468	0.32890
H3	0.15647	-0.10789	0.36867
C2	0.07045	-0.00261	0.39005
C3	-0.00313	-0.00731	0.33091
C4	-0.06887	-0.00319	0.34546
C5	-0.14669	-0.00150	0.28191
H4	-0.18428	-0.03320	0.30145
H5	-0.14746	-0.07814	0.24308
H6	-0.15762	0.10820	0.26079
C6	-0.00703	-0.00905	0.25093
C7	-0.03266	0.12658	0.20252
H7	-0.05335	0.21788	0.21757
C8	-0.02744	0.12542	0.13253
H8	-0.04497	0.21746	0.10109
C9	0.01584	-0.14434	0.22157
H9	0.02811	-0.24237	0.24930
C10	0.02082	-0.13662	0.15109
H10	0.03833	-0.22884	0.13327
N1	0.00120	0.00000	0.10795
Cu3	0.50000	0.00000	0.00000
O3	0.40081	0.00000	-0.07815
O4	0.45278	0.00000	0.07591
C11	0.36905	-0.00299	0.13774
H11	0.41117	-0.05585	0.17680
H12	0.32345	-0.06468	0.12937
H13	0.36343	0.10789	0.15315
C12	0.38326	0.00261	0.06637
C13	0.32319	0.00731	-0.00658
C14	0.33657	0.00319	-0.07286
C15	0.27204	0.00150	-0.14999
H14	0.29086	0.03320	-0.18808

Atom	*x*	*y*	*z*
H15	0.23339	0.07814	-0.15011
H16	0.25084	-0.10820	-0.16062
C16	0.24354	0.00905	-0.00915
C17	0.19494	-0.12658	-0.03410
H17	0.20957	-0.21788	-0.05514
C18	0.12538	-0.12542	-0.02769
H18	0.09381	-0.21746	-0.04477
C19	0.21471	0.14434	0.01431
H19	0.24251	0.24237	0.02617
C20	0.14466	0.13662	0.02049
H20	0.12722	0.22884	0.03838
N2	0.10140	0.00000	0.00150

Table S3. Modified Dubinin–Astakhov (MDA) isotherm fitting parameters, and micropore volumes calculated from CO_2 desorption data for $[Cu_2(Cu(pyac)_2)_2(SiF_6)]_n$.

Temp. (° C)	Equil. Time Interval (s)	MDA isotherm parameters						V_{mp} ($cm^3\ g^{-1}$)
		q_o ($mmol\ g^{-1}$)	C $(-)$	K ($mmol\ g^{-1}\ atm^{-1}$)	α $(-)$	n $(-)$	std. dev.[a]	
-78.5	20	5.827	0.250	0.109	9.780	0.471	0.069	0.218
25	20	6.336	0.231	1.111	249.930	2.059	0.041	0.395
	50	7.902	0.226	0.200	519.230	1.622	0.052	0.493
	100	8.453	0.195	5.057	8255.655	2.102	0.061	0.527
0	20	10.892	0.283	0.109	9.780	1.083	0.037	0.679

[a] Standard deviation was estimated from the sum of the squares of the residuals between the observed and calculated adsorbed amount values.

Table S4. Dual-site Langmuir-Freundlich isotherm model fit parameter CO_2 or CH_4 adsorption onto $[Cu_2(Cu(pyac)_2)_2(SiF_6)]_n$ at 25 °C.

Adsorbate	$q_{sat,A}$ ($mmol\ g^{-1}$)	b_A (atm^{-1})	α_A $(-)$	$q_{sat,B}$ ($mmol\ g^{-1}$)	b_B (atm^{-1})	α_B $(-)$
CO_2	5.8394	0.0236	3.3866	2.8262	0.7149	1.0319
CH_4	0.2071	0.6577	3.5381	0.2378	3.0811	1.3032

Table S5. Comparison of adsorption capacity and IAST selectivity of selected pillared-layered PCPs having 1D pore galleries. Selectivity corresponds to a CO_2/CH_4 (50:50) molar-based mixture at 25 °C and 1 atm.

Adsorbent	Effective Pore Size (Å)	BET Surface Area ($m^2\ g^{-1}$)	CO_2 Uptake (mmol g^{-1})	$-\Delta H_{ads}$ (kJ mol^{-1})	S_{IAST} (--)	Refs
$[Cu(Cu(pyac)_2)_2(SiF_6)]_n$	20.2	463	1.29	21	9.1	This work
$[Cu(bpy)_2(SiF_6)]_n$	9.5	1468	5.14	27	10.1	[13]
$[Cu(pia)_2(SiF_6)]_n$	12.0	285	1.24	30	10.1	[14]
$[Cu(bpe)_2(SiF_6)]_n$	12.5	2718	2.72	21	7.6	[13]
$[Cu(dpa)_2(SiF_6)]_n$	13.0	3140	1.15	22	5.0	[15]
$[Cu(dpa)_2(SiF_6)]_n$-i	5.1	735	5.81	32	33.2	[15]
$[Cu_2(pzdc)_2(bpe)]_n$	10.3 × 6.0	846	1.10	26	4.7	[16]
$Zn_2(bdc)_2(dabco)$	12.0 x 15.2	1911	2.06	22	4.9	[17]
$[Cu_2(tcmb)(bpp)(\mu_3\text{-}OH)]_n$	6.0 × 3.4	808	2.00	27	4.0	[18]

Notes:

- The effective window size of the one-dimensional channels of the SIFSIX MOFs is the diagonal distance between fluor atoms calculated from the crystallographic structures considering the van der Waals radii.
- The effective window size of the one-dimensional channels of the other materials is the channel dimensions considering the van der Waals radii.
- *Abbreviations: bpy* = 4,4′-bipyridine; *pia* = *N*-(pyridin-4-yl)isonicotinamide; *bpe* = 1,2-bis(4- pyridyl)ethene; *dpa* = 4,4'-dipyridylacetylene; *pyac* = 3-(4-pyridyl)pentane-2,4-dionato; *pzdc* = pyrazine-2,3-dicarboxylate; *bdc* = 1,4-benzene dicarboxylate; *dabco* = 1,4-diazabicyclo[2.2.2]octane*; tcmbt* = N,N′,N″-tris(carboxymethyl)-1,3,5-benzenetricarboxamide; bpp = 1,3-bis(4-pyridyl)propane.

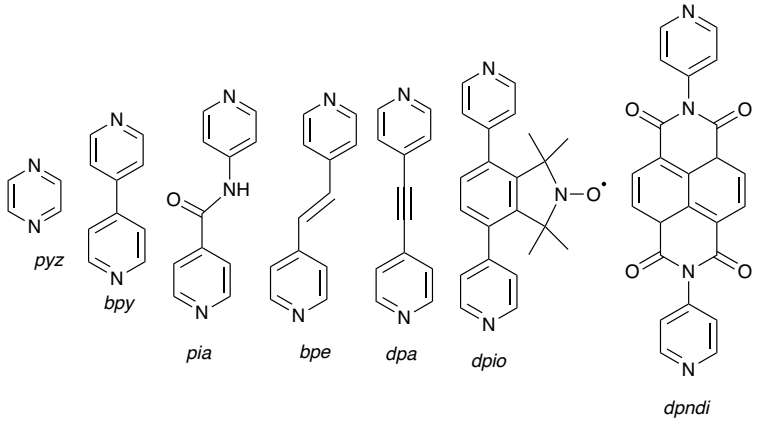

Chart S1. Some linkers reported in the literature to construct SIFSIX MOFs. Abbreviations: *pyz* = pyrazine; *bpy* = 4,4′-bipyridine; *pia* = *N*-(pyridin-4-yl)isonicotinamide; *bpe* = 1,2-bis(4-pyridyl)ethene; *dpa* = 4,4'-dipyridylacetylene; *dpio* = 4,7-bis(4-pyridyl)-1,1,3,3-tetramethylisoindolin-2-yloxyl; *dpndi* = *N,N*′-di(4-pyridyl)-1,4,5,8-naphthalene diimide.

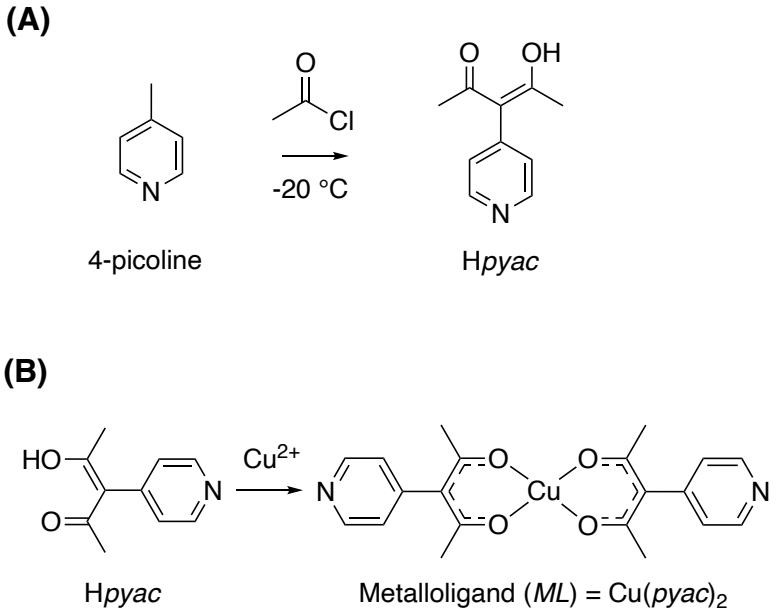

Scheme S1. Synthesis routes to yield (A) the organic linker 3-(4-pyridyl)pentane-2,4dione (H*pyac*) and (B) the diketonate metalloligand bis[3-(4-pyridyl)pentane-2,4-dionato]copper(II) (Cu(*pyac*)$_2$).

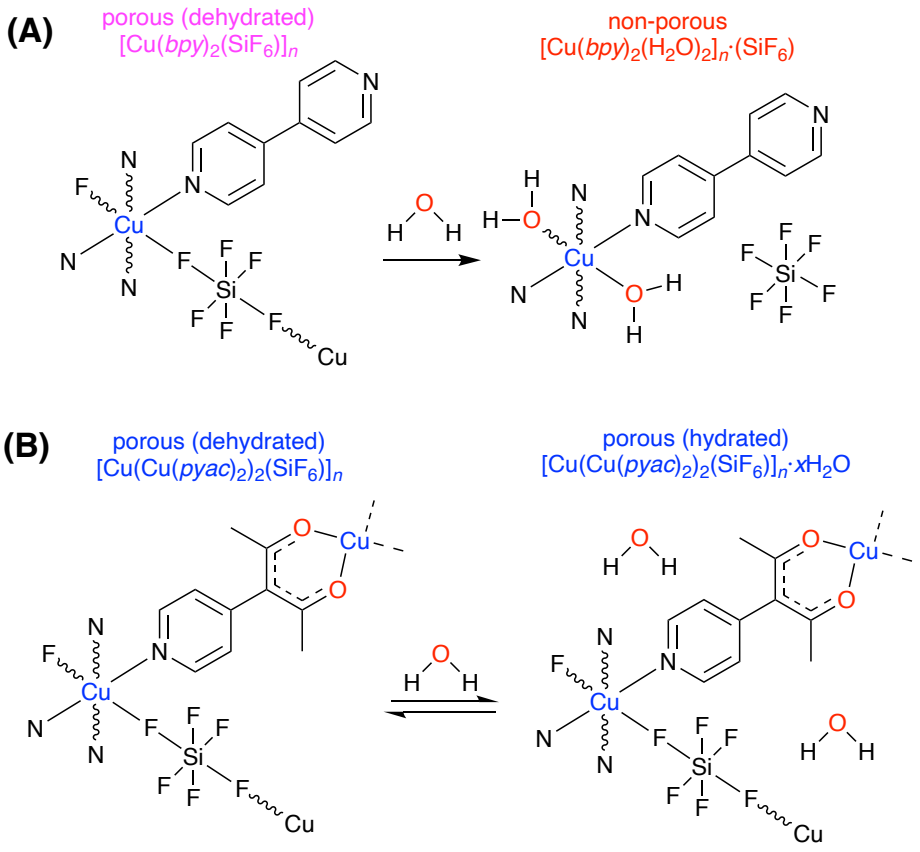

Scheme S2. (A) Irreversible phase transformation from porous $[Cu(bpy)_2(SiF_6)]_n$ to non-porous $[Cu(bpy)_2(H_2O)_2]_n\cdot(SiF_6)$ and (B) reversible adsorption and desorption of water in $[Cu(Cu(pyac)_2)_2(SiF_6)]_n$.

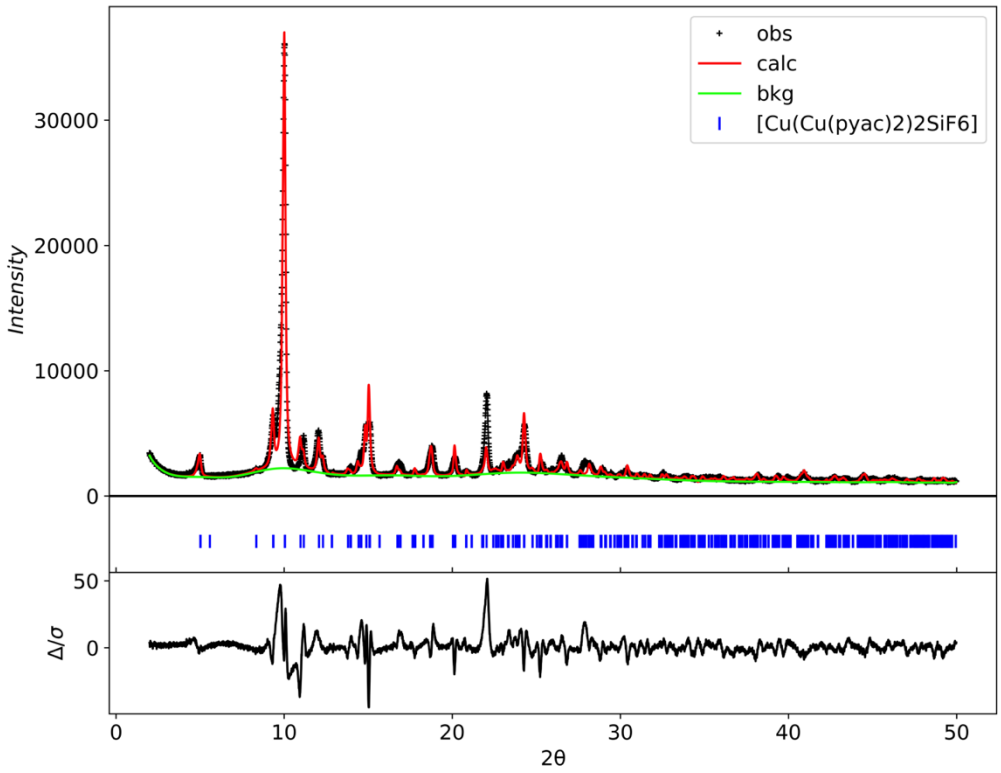

Figure S1. Observed (black crosses) and calculated (red line) powder X-ray diffraction patterns and difference profile for the Rietveld refinement of $[Cu_2(Cu(pyac)_2)_2(SiF_6)]_n$ without guest molecules. The blue vertical line markers shown below the profile correspond to the Bragg positions. The scanned range from 2 to 50 deg (2θ) was selected for the Rietveld refinement as no significant peaks were observed at higher angles.

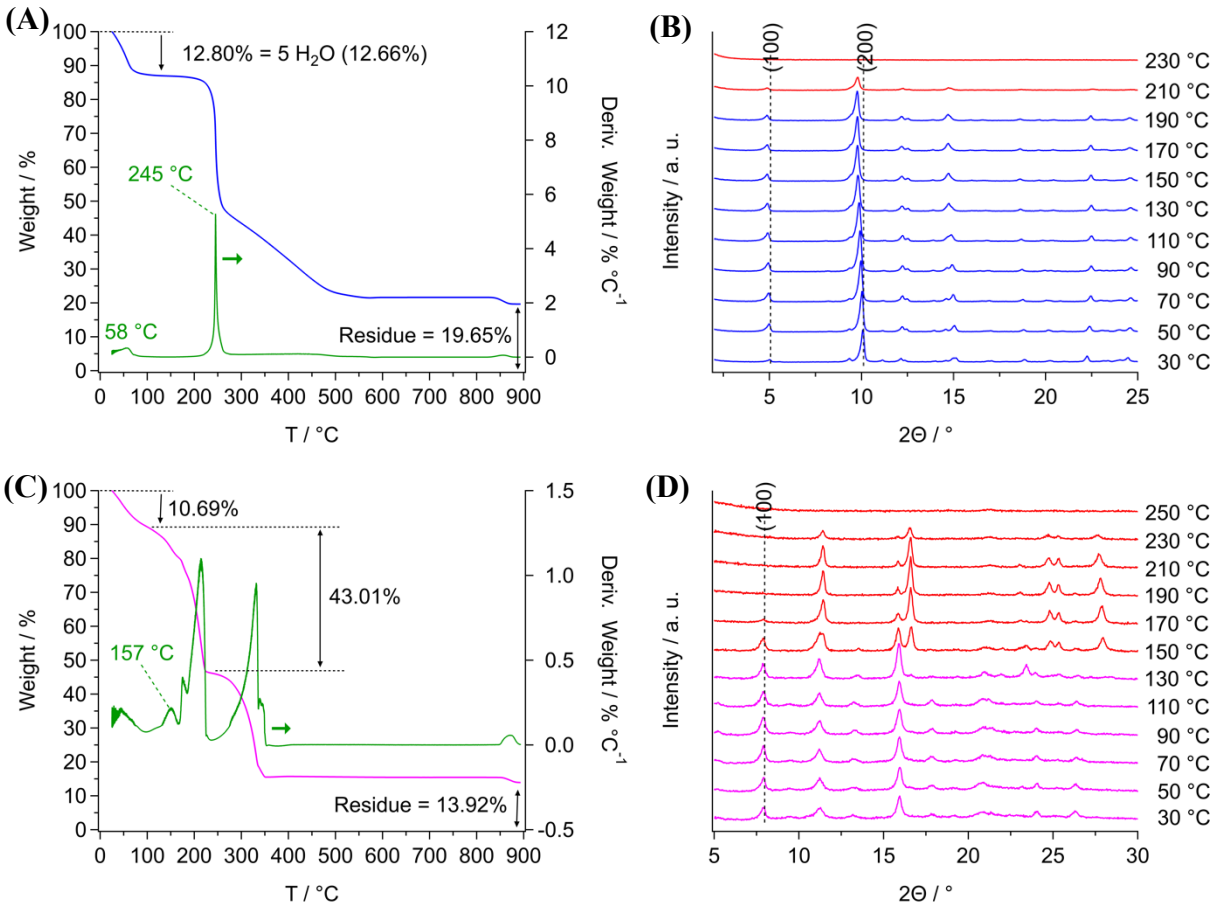

Figure S2. Thermal gravimetric analysis profiles for as-synthesized (A) $[Cu_2(Cu(pyac)_2)_2(SiF_6)\cdot 5H_2O]_n$ and (C) $[Cu_2(bpy)_2(SiF_6)\cdot xH_2O]_n$ under N_2 gas flowing at 60 mL min^{-1} and a heating ramp of 10 °C min^{-1}. In situ high-temperature XRD patterns for (B) $[Cu_2(Cu(pyac)_2)_2(SiF_6)]_n$ and (D) $[Cu_2(bpy)_2(SiF_6)]_n$ under He gas flowing at 60 mL min^{-1} and a scan rate of 1° min^{-1}.

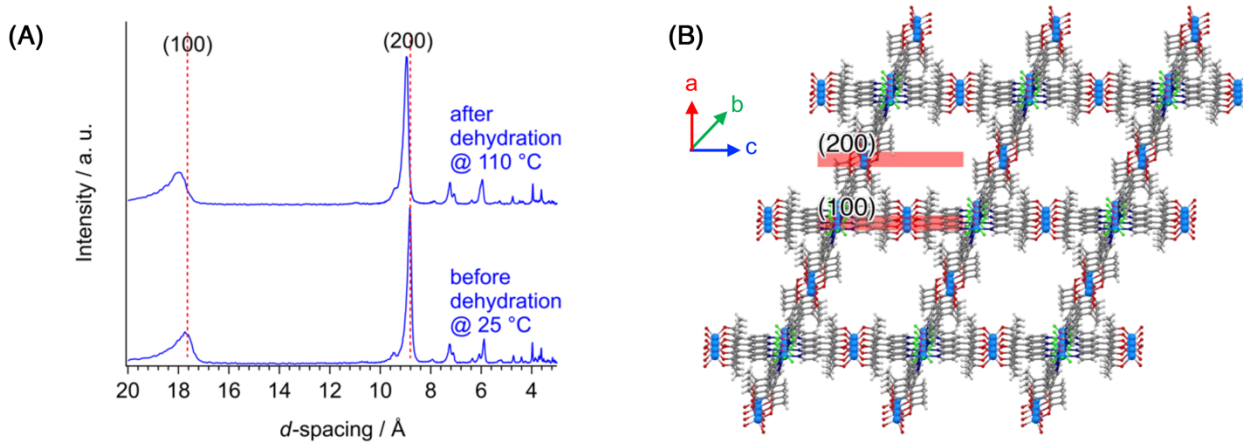

Figure S3. (A) Structural view of the (100) and (200) crystallographic planes of $[Cu(Cu(pyac)_2)_2(SiF_6)]_n$ which are parallel to the *bc* planes and (B) Detailed view of the XRD of $[Cu(Cu(pyac)_2)_2(SiF_6)]_n$ showing the peak shifting for the (100) and (200) crystallographic planes upon dehydration. Colour code: Cu (sky blue), Si (magenta), F (green), O (red), C (grey), H (white), N (navy blue).

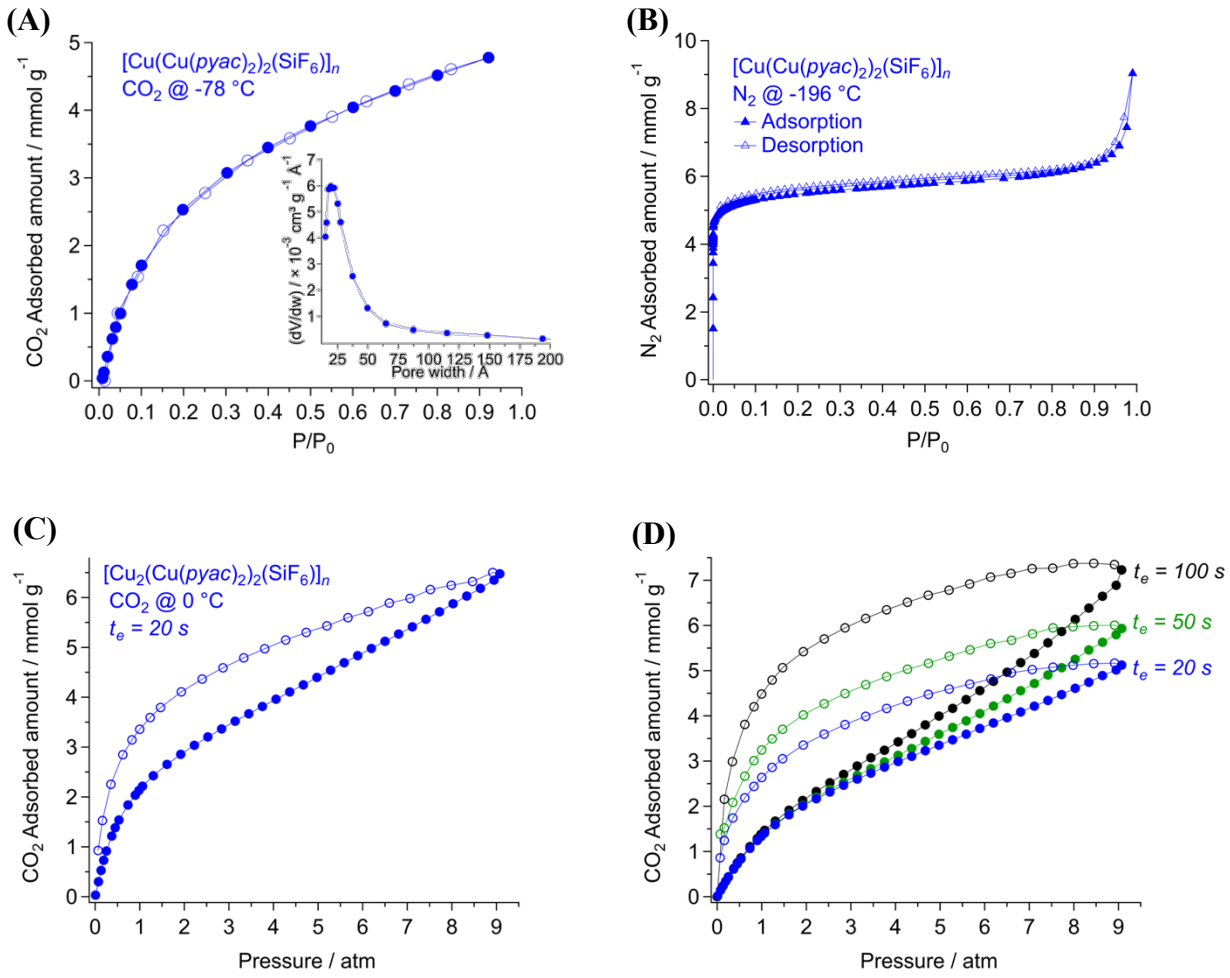

Figure S4. Single-component adsorption (filled symbols) and desorption (empty symbols) isotherms over $[Cu(Cu(pyac)_2)_2(SiF_6)]_n$ for (A) CO_2 at -78 °C (the inset shows a Horvath-Kawazoe differential pore volume plot), (B) N_2 at -196 °C, (C) CO_2 at 0 °C, and (D) CO_2 at 25 °C and different equilibration time intervals.

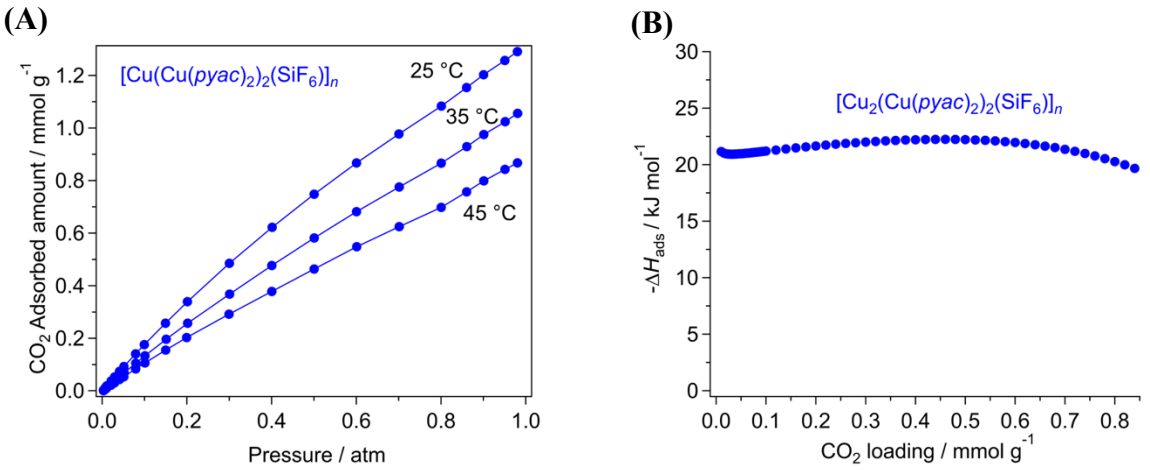

Figure S5. (A) Equilibrium isotherms for CO_2 adsorption gathered at 25, 35, and 45 °C over $[Cu(Cu(pyac)_2)_2(SiF_6)]_n$. (B) Isosteric heat profile of CO_2 over $[Cu(Cu(pyac)_2)_2(SiF_6)]_n$.

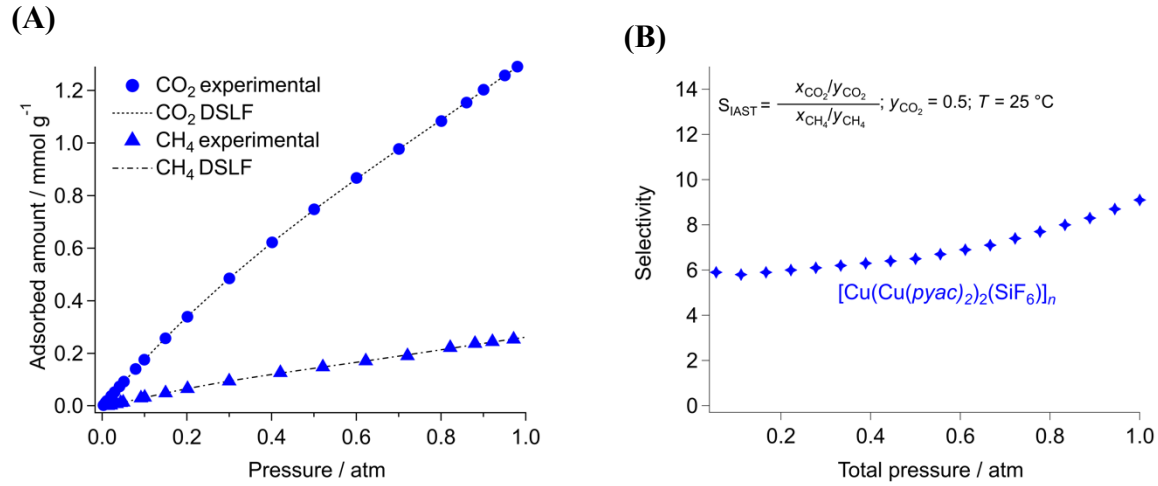

Figure S6. (A) Equilibrium isotherms for single component CO_2 and CH_4 adsorption onto $[Cu(Cu(pyac)_2)_2(SiF_6)]_n$ (dashed lines represent data fits with DSFL models). (B) Adsorption selectivity for CO_2/CH_4 equimolar gas mixture on $[Cu(Cu(pyac)_2)_2(SiF_6)]_n$ at 25 °C based on the Ideal Adsorbed Solution Theory (IAST) and single-component equilibrium adsorption data for the adsorbates.

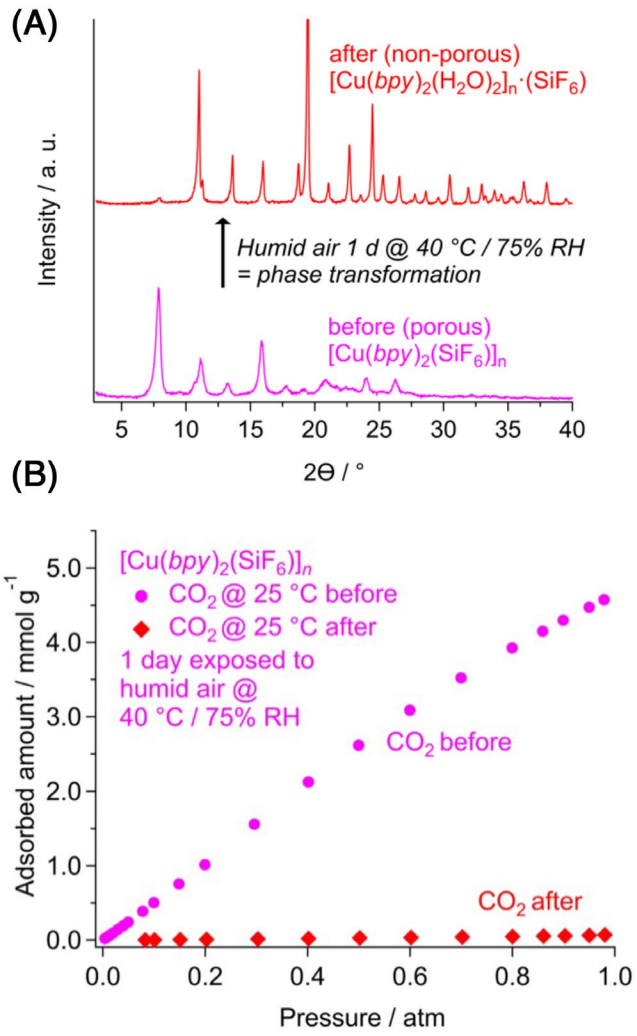

Figure S7. (A) Powder X-ray diffraction patterns before and after humidity tests, and (B) equilibrium isotherms for single component CO_2 adsorption before and after exposure to humidity for $[Cu(bpy)_2(SiF_6)]_n$. XRD data were gathered at ambient temperature.

References

(1) Mackay, L. G.; Anderson, H. L.; Sanders, J. K. M., A platinum-linked porphyrin trimer and a complementary aluminium tris[3-(4-pyridyl)acetylacetonate] guest. *Journal of the Chemical Society, Perkin Transactions 1* **1995**, 2269-2273.

(2) Zhang, Y.; Chen, B.; Fronczek, F. R.; Maverick, A. W., A Nanoporous Ag−Fe Mixed-Metal−Organic Framework Exhibiting Single-Crystal-to-Single-Crystal Transformations upon Guest Exchange. *Inorganic Chemistry* **2008,** *47*, 4433-4435.

(3) S. Turner, S.; Collison, D.; E. Mabbs, F.; Halliwell, M., Preparation, magnetic properties and crystal structure of bis[3-(4-pyridyl)pentane-2,4-dionato]copper(II). *J. Chem. Soc., Dalton Trans.* **1997**, 1117-1118.

(4) Lavrenyuk, H.; Kochubei, V.; Mykhalichko, O.; Mykhalichko, B., Development and thermal behavior of a new type of polymer materials with reduced combustibility based on epoxy–amine composites modified with copper(II) hexafluorosilicate. *Journal of Thermal Analysis and Calorimetry* **2022,** *147*, 2197-2207.

(5) Elsaidi, S. K.; Venna, S. R.; Mohamed, M. H.; Gipple, M. J.; Hopkinson, D. P., Dual-Layer MOF Composite Membranes with Tuned Interface Interaction for Postcombustion Carbon Dioxide Separation. *Cell Reports Physical Science* **2020,** *1*, 100059.

(6) Blanton, J. R.; Papoular, R. J.; Louër, D., PreDICT: a graphical user interface to the DICVOL14 indexing software program for powder diffraction data. *Powder Diffraction* **2019,** *34*, 233-241.

(7) Toby, B. H.; Von Dreele, R. B., GSAS-II: the genesis of a modern open-source all purpose crystallography software package. *Journal of Applied Crystallography* **2013,** *46*, 544-549.

(8) Cheng, L. S.; Ralph T, Y., Improved Horvath—Kawazoe equations including spherical pore models for calculating micropore size distribution. *Chem. Eng. Sci.* **1994,** *49*, 2599-2609.

(9) Kapoor, A.; Ritter, J. A.; Yang, R. T., On the Dubinin-Radushkevich equation for adsorption in microporous solids in the Henry's law region. *Langmuir* **1989,** *5*, 1118-1121.

(10) Nuhnen, A.; Janiak, C., A practical guide to calculate the isosteric heat/enthalpy of adsorption via adsorption isotherms in metal–organic frameworks, MOFs. *Dalton Trans.* **2020,** *49*, 10295-10307.

(11) Myers, A. L.; Prausnitz, J. M., Thermodynamics of mixed-gas adsorption. *AlChE J.* **1965,** *11*, 121-127.

(12) Toby, B. H., R factors in Rietveld analysis: How good is good enough? *Powder Diffraction* **2006,** *21*, 67-70.

(13) Burd, S. D.; Ma, S.; Perman, J. A.; Sikora, B. J.; Snurr, R. Q.; Thallapally, P. K.; Tian, J.; Wojtas, L.; Zaworotko, M. J., Highly Selective Carbon Dioxide Uptake by [Cu(bpy-n)2(SiF6)] (bpy-1 = 4,4′-Bipyridine; bpy-2 = 1,2-Bis(4-pyridyl)ethene). *J. Am. Chem. Soc.* **2012,** *134*, 3663-3666.

(14) Xiong, S.; He, Y.; Krishna, R.; Chen, B.; Wang, Z., Metal–Organic Framework with Functional Amide Groups for Highly Selective Gas Separation. *Cryst. Growth Des.* **2013,** *13*, 2670-2674.

(15) Nugent, P.; Belmabkhout, Y.; Burd, S. D.; Cairns, A. J.; Luebke, R.; Forrest, K.; Pham, T.; Ma, S.; Space, B.; Wojtas, L.; Eddaoudi, M.; Zaworotko, M. J., Porous materials with optimal adsorption thermodynamics and kinetics for CO2 separation. *Nature* **2013,** *495*, 80-84.

(16) Chen, H.; Riascos-Rodríguez, K.; Marcano-González, M. E.; Hernández-Maldonado, A. J., Cu2(pzdc)2L [L=dipyridyl-based ligands] porous coordination polymers: Hysteretic adsorption and diffusion kinetics of CO2 and CH4. *Chemical Engineering Journal* **2016,** *283*, 806-815.

(17) Zhou, K.; Chaemchuen, S.; Wu, Z.; Verpoort, F., Rapid room temperature synthesis forming pillared metal-organic frameworks with Kagomé net topology. *Microporous and Mesoporous Materials* **2017,** *239*, 28-33.

(18) Lu, Z.; Xing, H.; Sun, R.; Bai, J.; Zheng, B.; Li, Y., Water Stable metal–organic framework evolutionally formed from a flexible multidentate ligand with acylamide groups for selective CO_2 adsorption. *Cryst. Growth Des.* **2012,** *12*, 1081-1084.